Remote Sensing of Environment 150 (2014) 66–81

Contents lists available at ScienceDirect

Remote Sensing of Environment

journal homepage: www.elsevier.com/locate/rse

Monitoring Everglades freshwater marsh water level using L-band synthetic aperture radar backscatter☆

Jin-Woo Kim [a,*], Zhong Lu [b], John W. Jones [c], C.K. Shum [a,d], Hyongki Lee [e], Yuanyuan Jia [a]

[a] Division of Geodetic Science, School of Earth Sciences, The Ohio State University, Columbus, OH, USA
[b] U.S. Geological Survey, Vancouver, WA, USA
[c] U.S. Geological Survey, Reston, VA, USA
[d] Institute of Geodesy and Geophysics, Chinese Academy of Sciences, China
[e] Department of Civil and Environmental Engineering, University of Houston, Houston, TX, USA

ARTICLE INFO

Article history:
Received 10 June 2013
Received in revised form 21 February 2014
Accepted 19 March 2014
Available online 14 May 2014

Keywords:
Everglades
SAR
InSAR
Backscatter coefficient
Wetland hydrology

ABSTRACT

The Florida Everglades plays a significant role in controlling floods, improving water quality, supporting ecosystems, and maintaining biodiversity in south Florida. Adaptive restoration and management of the Everglades requires the best information possible regarding wetland hydrology. We developed a new and innovative approach to quantify spatial and temporal variations in wetland water levels within the Everglades, Florida. We observed high correlations between water level measured at in situ gages and L-band SAR backscatter coefficients in the freshwater marsh, though C-band SAR backscatter has no close relationship with water level. Here we illustrate the complementarity of SAR backscatter coefficient differencing and interferometry (InSAR) for improved estimation of high spatial resolution water level variations in the Everglades. This technique has a certain limitation in applying to swamp forests with dense vegetation cover, but we conclude that this new method is promising in future applications to wetland hydrology research.

1. Introduction

Wetlands provide significant ecosystem services including flood control, water quality improvement, waterfowl and rare plant habitat provision, and unique recreational opportunities. However, almost half of the wetland area in the United States has been converted to other land uses, since major portions of the wetlands in the Louisiana, Mississippi, California, Florida, and Ohio have been utilized for agriculture, urban development and resource extraction (Fraser & Keddy, 2005; Mitsch & Gosselink, 2007). The Everglades of Florida are a unique ecosystem recognized by the United Nations Educational, Scientific and Cultural Organization (UNESCO) as a world heritage site. Everglades hydrology is the most important factor in establishing and maintaining the capacity of the wetlands to support the vegetation, animals and microbes that are closely linked to its hydroperiod and water level fluctuations. Alteration of Everglades hydrology by drainage canal and dike construction and the manipulation of flows for flood control, irrigation and other water uses has changed wetland conditions. Furthermore, the Everglades have been the subject of a major ecological restoration effort on the part of a coalition of government and non-government institutions. The fundamental goal of the project is to control the timing, quantity and quality of water flowing through the Everglades to replicate hydrologic conditions that existed prior to human intervention and development (NRC, 2001; SFERTF, 1998; Solecki et al., 1999; USACE, 1999). Various Federal and State agencies have installed water stage gages throughout the Everglades for research and monitoring purposes. Data from all these sources are now collected operationally, distributed and converted to water depths through the Everglades Depth Estimation Network or "EDEN" (Tellis, 2006). While the gage network is unique given its density over such a large wetland area, gages may malfunction during extreme flood or drought conditions. Improved monitoring of Everglades water levels are needed for scientific and resource management purposes (Jones et al., 2012). Information gathered through remote sensing can supplement processes to the understanding of development through field research to help restore and adaptively manage the Everglades (Jones, 2011).

Synthetic aperture radar (SAR) data comprises backscattering coefficient (called sigma naught; σ_0) as well as phase information. SAR interferometry (InSAR) using the phase information has traditionally been used to detect horizontal and vertical displacements by catastrophic natural disasters of earthquakes and volcanoes throughout the world (Hanssen, 2000; Lu, 2007; Tong, Sandwell, & Fialko, 2010), and

☆ This draft manuscript is distributed solely for purposes of scientific peer review. Its content is deliberative and predecisional, so it must not be disclosed of released by reviewers. Because the manuscript has not yet been approved for publication by the U.S. Geological Survey (USGS), it does not represent any official USGS finding or policy.

* Corresponding author at: Division of Geodesy and Geospatial Science, School of Earth Sciences, The Ohio State University, 275 Mendenhall Laboratory, 125 South Oval Mall, Columbus, OH 43210, USA. Tel.: +1 614 906 8884; fax: +1 614 292 7688.
E-mail address: kim.2364@osu.edu (J.-W. Kim).

http://dx.doi.org/10.1016/j.rse.2014.03.031
0034-4257/

groundwater depletion around major metropolitan areas such as Phoenix and Las Vegas (Amelung, Galloway, Bell, Zebker, & Laczniak, 1999; Casu, Buckley, Manzo, Pepe, & Lanari, 2005; Galloway & Hoffmann, 2007; Liu, Buckley, Ding, Chen, & Luo, 2009). However, innovative applications of InSAR to estimating hydrologic changes in the wetlands have also been successful. Since Alsdorf et al. (2000, 2001) mapped hydraulic flow in the Amazon basin using InSAR, Lu et al. (2005, 2008) showed the feasibility of C-band interferometry over the wetland in Louisiana, Wdowinski, Amelung, Miralles-Wilhelm, Dixon, and Carande (2004, 2008) detected surface water level changes within water conservation area in the Everglades, and Kim et al. (2009) combined radar altimetry and InSAR to estimate absolute water level changes in the swamp forests of the Atchafalaya basin. Interferometric coherence, a by-product of InSAR, may be the key component in distinguishing wetland types and other biogeological factors. Lee, Hong, Kim, Yamaguchi, and Won (2006) reported polarimetric features of the interaction between water and vertical wood structure, which are accounted for the ratio of double bounce to surface scattering. Hong, Wdowinski, Kim, and Won (2010) successfully measured the water level variations over the Everglades by applying STBAS (small temporal baseline subset) method to the RADARSAT-1 data. Kim et al. (in press) analyzed the relation between interferometric coherence in the Everglades wetland, inherent SAR parameters of polarization, incidence angle, and wavelength, wetland types, and physical and temporal InSAR components.

To-date, SAR backscatter coefficients from polarimetric or non-polarimetric spaceborne or airborne SAR platforms have mostly been employed for land cover classification, wind speed and direction estimation, and cryosphere monitoring. SAR backscattering coefficient in wetland studies has been very useful for discriminating land cover types, and delineating inundated areas in the large river basins or wetland areas (Hess, Melack, & Simonett, 1990; Hess, Melack, Filoso, & Wang, 1995; Hess, Melack, Novo, Barbosa, & Gastil, 2003; Ramsey, 1995; Wang, Hess, Filoso, & Melack, 1995; Kwoun & Lu, 2009; Rebelo, 2010; Betbeder et al., 2014). However, only a few studies have focused on the variation of radar backscatter associated with wetland water level changes (Smith, 1997). Hess et al. (1995),Alsdorf et al. (2000) andAlsdorf, Smith, and Melack (2001) showed that variations in flood stages along the Brazilian Amazon influenced the radar backscatter signatures from the SIR-C instruments. Frappart, Seyler, Martinez, León, and Cazenave (2005) combined water extent from SAR images with altimetry-based water levels to estimate water level maps of wetlands in a sub-basin of the Amazon. Kasischke et al. (2003) studied the relationship of ERS C-band radar backscatter and several components including water level change, biomass, and soil moisture over the Big Cypress National Preserve in the Everglades. One obstacle to wider use of SAR/InSAR in wetland applications is the lack of water level gage data inside wetland for example, to provide vertical datum constraints. Most gages are located in open water and near-shore, where SAR produces little backscatter and it is therefore difficult to establish any concrete relationship between hydrologic change and backscatter. However, given the EDEN's extensive water monitoring stations, the Everglades is an ideal place for the study to correlate wetland water level changes with SAR backscatter.

In this study, we analyzed relationships among SAR backscatter coefficient, InSAR differential interferograms, and in situ water level changes to test the possibility whether the water level changes can be estimated from SAR backscatter and the extensive hydrological monitoring using the spaceborne SAR data is available over wetland areas. Thirty-eight

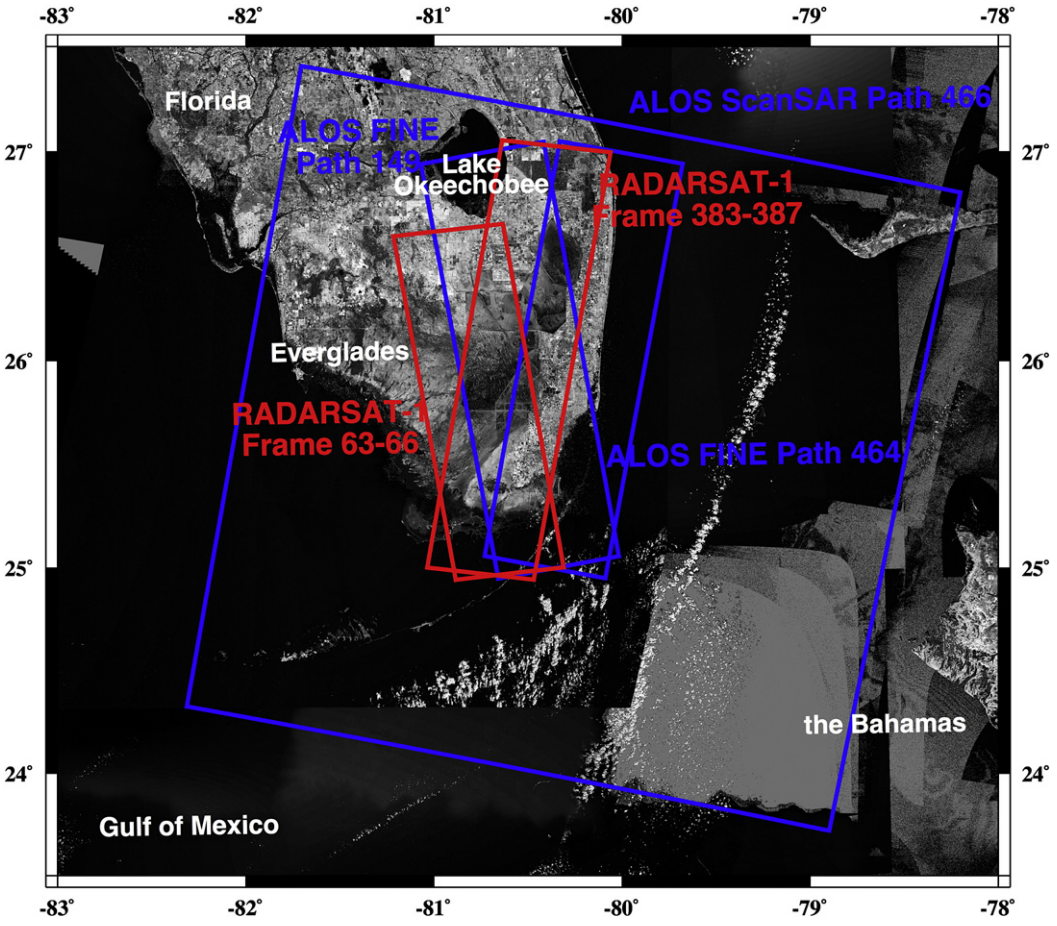

Fig. 1. Landsat image including the research region shows the coverage of ALOS fine-beam and ScanSAR mode (blue boxes) and RADARSAT-1 imagery (red boxes).

gages installed in the Everglades freshwater marshes provide daily water level data, which can be used to compare with possible water level changes inferred by the backscattering coefficients and interferograms derived from L-band PALSAR fine-beam mode (FB) and ScanSAR data, and C-band Radarsat-1 SAR data. We will compare the respective temporal and spatial variations on water level changes using the different types (ALOS PALSAR and Radarsat-1) of SAR backscatters with C- and L-band frequencies in the Everglades.

2. Characteristics of study region and data

2.1. Characteristics of study region

The Florida wetlands south of Lake Okeechobee (Fig. 1) are collectively referred to as the Everglades. Historically, this "river of grass" flowed from Lake Okeechobee south/southwestward to the Florida Bay (Douglas, 1947). Beginning in the 19th Century, canals, levees,

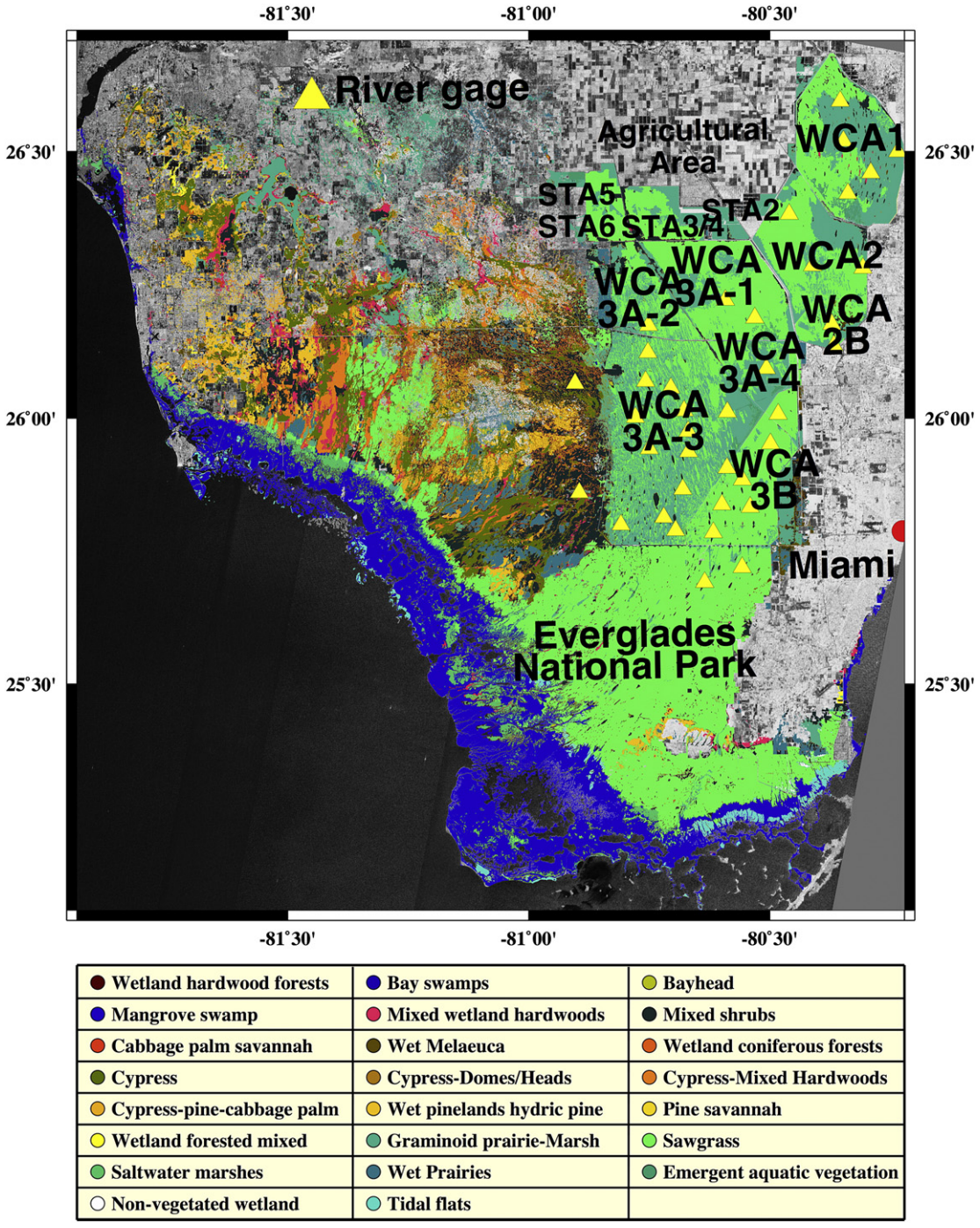

Wetland hardwood forests	Bay swamps	Bayhead
Mangrove swamp	Mixed wetland hardwoods	Mixed shrubs
Cabbage palm savannah	Wet Melaeuca	Wetland coniferous forests
Cypress	Cypress-Domes/Heads	Cypress-Mixed Hardwoods
Cypress-pine-cabbage palm	Wet pinelands hydric pine	Pine savannah
Wetland forested mixed	Graminoid prairie-Marsh	Sawgrass
Saltwater marshes	Wet Prairies	Emergent aquatic vegetation
Non-vegetated wetland	Tidal flats	

Fig. 2. Land classification map (USACE, 1999) in the wetlands of the Everglades, Florida. Each colored region represents vegetation types and the classification map includes inland and coastal marshes, and swamp forests. The map also shows the location of thirty-eight gages (yellow triangles) and each section of Water Conservation Areas (WCA1, WCA2, WCA2B, WCA3A-1–4, WCA3B) and Stormwater Treatment Area (STA2–6). Background gray image is an intensity data from ALOS PALSAR ScanSAR mode. Individual WCAs are dissected by control structures resulting in such as WCA2, WCA2B, WCA3A, and WCA3B. Because WCA3A is separated by large canals, we divided the WCA3A into WCA3A-1–4 for better description. The density of installed gages varies by WCA section. WCA1, WCA3A-3, and WCA3B have densely spaced gages compared to other WCA subsections.

and roads were constructed to drain sawgrass prairie for agricultural uses, control flooding from the Lake, supply water for irrigation, industry and residential use and afford population growth and commerce. Now these canals, levees, roads and other administrative boundaries divide the Everglades into water conservation areas (WCAs), the Big Cypress National Preserve, the Biscayne National Park, the Everglades National Park, and the Florida Panther National Wildlife Refuge (among others). The Everglades consists of herbaceous and woody wetlands also called freshwater marshes and swamps (Doren, Rutchey, & Welch, 1999; Kim et al., in press). The dominant plant species of WCAs and Everglades National Park is sawgrass and graminoid-prairie (cattail; *typha*). Hardwood forests, pineland savannas, and cypress forests comprise the woody wetlands (Fig. 2). The freshwater marsh is dotted with tree islands composed of mixed shrubs in a slightly high elevation. The regions in the west of the WCAs are occupied by freshwater swamp, which is characterized by seasonally inundated Cypress forests reaching the height of tens of meters. The coastal regions around the Florida Bay and Gulf of Mexico are covered by Mangrove swamps. In this study, we concentrated on the WCAs, because they include a large number of water monitoring stations, the paths of various satellite SAR systems overlap there, and the region is one of planned road/levee alteration for ecosystem restoration (USACE, 1999).

The dominant vegetation cover in the Water Conservation Areas (WCA1–3) and Stormwater Treatment Areas (STA2–6) is *Cladium jamaiscense* or "sawgrass" (Zweig & Kitchens, 2008) (Fig. 2). Due to the water flow manipulation via the South Florida Water Management District (SFWMD) control system, each WCA and even subsections within them can show very different hydrologic patterns even given similar weather conditions.

2.2. SAR data

We combined 7 ALOS PALSAR ScanSAR scenes, providing large coverage (350 km × 350 km) with 18 PALSAR Fine Beam (FB) mode scenes (blue box in Fig. 1), offering high resolution of 30 m in ground, to have sufficient temporal and spatial resolution with ALOS 46 day orbit to uniquely water level changes within the Everglades. One intriguing advantage given the use of different beam modes is that ScanSAR (100 meter resolution in ground) and FB data are acquired using descending and ascending tracks, respectively. Because they observe the same area with different perspectives, the radar backscatter can be affected by different penetration and backscattering within a resolution cell. Different or even independent signatures from identical land surfaces may add diagnostic information. In addition to the ALOS PALSAR data, 33 FB Radarsat-1 images (red box in Fig. 1) were also analyzed. Their spatial resolution is approximately 30 m following multi-look processing and geocoding. ALOS ScanSAR has the largest coverage among all used scenes. Only the third and fourth subswaths among the total five available from ScanSAR needed to be merged into a single SAR backscatter image, because both have enough coverage over the Everglades. The FB scenes of ALOS and Radarsat-1 either partially or completely cover our research region (Table 1). PALSAR scenes from path 149 (FB) were observed from ascending track, and those from paths 464 (FB) and 466 (ScanSAR) were acquired from descending track. Radarsat-1 scenes were obtained from both descending and ascending tracks. We only utilized HH-polarized ALOS PALSAR and Radarsat-1 imagery in this study because the HH-polarized radar has a strong double bounce signal associated with tree-trunks in swamp forests and grass stems in freshwater marsh, and because HH-polarized signal is less attenuated by vertical stems or trunks in the wetlands due to larger

Table 1
List of used ALOS PALSAR and Radarsat-1 scenes.

Date	Sensor	Path	Beam	Band	Incidence angle (°)	Direction	Date	Sensor	Frame	Beam	Band	Incidence angle (deg)	Direction
2007.01.11	PALSAR	149	Fine	L-band	38.74	Ascending	2007.01.24	Radarsat-1	383–387	Fine-5	C-band	46.85	Descending
2008.01.14	PALSAR	149	Fine	L-band	38.74	Ascending	2007.02.17	Radarsat-1	383–387	Fine-5	C-band	46.85	Descending
2008.05.31	PALSAR	149	Fine	L-band	38.74	Ascending	2007.03.13	Radarsat-1	383–387	Fine-5	C-band	46.85	Descending
2009.10.19	PALSAR	149	Fine	L-band	38.76	Ascending	2007.04.30	Radarsat-1	383–387	Fine-5	C-band	46.85	Descending
2010.01.19	PALSAR	149	Fine	L-band	38.74	Ascending	2007.05.24	Radarsat-1	383–387	Fine-5	C-band	46.86	Descending
2010.04.21	PALSAR	149	Fine	L-band	38.75	Ascending	2007.06.17	Radarsat-1	383–387	Fine-5	C-band	46.85	Descending
2010.06.06	PALSAR	149	Fine	L-band	38.74	Ascending	2007.07.11	Radarsat-1	383–387	Fine-5	C-band	46.86	Descending
2010.09.06	PALSAR	149	Fine	L-band	38.74	Ascending	2007.08.04	Radarsat-1	383–387	Fine-5	C-band	46.85	Descending
2010.12.07	PALSAR	149	Fine	L-band	38.74	Ascending	2007.08.28	Radarsat-1	383–387	Fine-5	C-band	46.86	Descending
2011.01.22	PALSAR	149	Fine	L-band	38.74	Ascending	2007.09.21	Radarsat-1	383–387	Fine-5	C-band	46.85	Descending
2011.03.09	PALSAR	149	Fine	L-band	38.73	Ascending	2007.10.15	Radarsat-1	383–387	Fine-5	C-band	46.85	Descending
2007.11.02	PALSAR	464	Fine	L-band	38.77	Descending	2007.11.08	Radarsat-1	383–387	Fine-5	C-band	46.86	Descending
2009.11.04	PALSAR	464	Fine	L-band	38.78	Descending	2007.12.02	Radarsat-1	383–387	Fine-5	C-band	46.86	Descending
2008.12.20	PALSAR	464	Fine	L-band	38.77	Descending	2007.12.26	Radarsat-1	383–387	Fine-5	C-band	46.86	Descending
2009.03.22	PALSAR	464	Fine	L-band	38.77	Descending	2008.01.19	Radarsat-1	383–387	Fine-5	C-band	46.86	Descending
2009.11.07	PALSAR	464	Fine	L-band	38.77	Descending	2007.02.12	Radarsat-1	383–387	Fine-5	C-band	46.86	Descending
2010.02.07	PALSAR	464	Fine	L-band	38.77	Descending	2008.03.07	Radarsat-1	383–387	Fine-5	C-band	46.86	Descending
2010.03.25	PALSAR	464	Fine	L-band	38.77	Descending	2008.03.31	Radarsat-1	383–387	Fine-5	C-band	46.86	Descending
2010.01.26	PALSAR	466	ScanSAR	L-band	34.53	Descending	2008.04.24	Radarsat-1	383–387	Fine-5	C-band	46.86	Descending
2010.03.13	PALSAR	466	ScanSAR	L-band	34.54	Descending	2007.01.18	Radarsat-1	63–66	Fine-5	C-band	46.03	Ascending
2010.04.28	PALSAR	466	ScanSAR	L-band	34.53	Descending	2007.03.07	Radarsat-1	63–66	Fine-5	C-band	46.03	Ascending
2010.07.29	PALSAR	466	ScanSAR	L-band	34.53	Descending	2007.03.31	Radarsat-1	63–66	Fine-5	C-band	46.03	Ascending
2010.09.13	PALSAR	466	ScanSAR	L-band	34.53	Descending	2007.05.18	Radarsat-1	63–66	Fine-5	C-band	46.03	Ascending
2010.12.14	PALSAR	466	ScanSAR	L-band	34.53	Descending	2007.06.11	Radarsat-1	63–66	Fine-5	C-band	46.03	Ascending
2011.01.29	PALSAR	466	ScanSAR	L-band	34.54	Descending	2007.07.05	Radarsat-1	63–66	Fine-5	C-band	46.03	Ascending
							2007.08.22	Radarsat-1	63–66	Fine-5	C-band	46.03	Ascending
							2007.09.15	Radarsat-1	63–66	Fine-5	C-band	46.03	Ascending
							2007.10.09	Radarsat-1	63–66	Fine-5	C-band	46.02	Ascending
							2007.11.26	Radarsat-1	63–66	Fine-5	C-band	46.03	Ascending
							2008.02.06	Radarsat-1	63–66	Fine-5	C-band	46.03	Ascending
							2008.03.01	Radarsat-1	63–66	Fine-5	C-band	46.03	Ascending
							2008.03.25	Radarsat-1	63–66	Fine-5	C-band	46.03	Ascending
							2008.04.18	Radarsat-1	63–66	Fine-5	C-band	46.03	Ascending

Fresnel reflection of HH than that of VV (Kim et al., 2009, in press). Therefore, HH-polarization is preferred over other polarized SAR data for SAR/InSAR, in terms of high coherence in InSAR and the sensitivity to the flooded and unflooded conditions in SAR radar backscatter (Kim et al., 2009).

2.3. Land cover and gage data

Land cover data (SFWMD, 2004) (Fig. 2) were used to identify vegetation types and verify that all water level gages were located within the wetland and not within a canal. The land cover data was created and revised by the SFWMD using visual interpretation of color infrared digital orthophotoquads produced from imagery acquired from November 2004 through March 2005. The vector data from high-resolution photogrammetry provides the detailed information enough to extract the land cover in the location of each gage. Water level gage data at locations (Fig. 2) assembled and quality assured through the EDEN were acquired from the U.S. Geological Survey (USGS) National Water Information system for Florida (http://waterdata.usgs.gov/fl/nwis), using EDEN with the North American Vertical Datum of 1988 (NAVD 88). The gages are located in the mixed shrubs, graminoid prairie marsh, and sawgrass marsh of the WCAs (Fig. 2). Note that the mixed shrubs-covered wetland is within the freshwater swamp, while most gages are in the freshwater marsh. Additional geospatial data such as the Shuttle Radar Topography Mission (SRTM) digital elevation model (DEM) and Landsat Thematic Mapper (TM) data were used for geocoding.

3. Data processing and methodology

ALOS PALSAR and Radarsat-1 raw signal data were converted into geocoded intensity imagery through signal processing and geocoding, such that we can uniquely analyze differences in reflective properties for the same pixel location on the ground but collected from different look angles and at different times. We used the full aperture algorithm (Cumming and Wong, 2005) with ALOS ScanSAR scenes, and filled gaps between bursts by zero padding, and implements conventional stripmap processors including focusing and range migration compensation. The intensity images from ALOS and Radarsat-1 FB were generated from the stripmap processor, which is also called the Range–Doppler Algorithm (RDA) (Curlander & McDonough, 1991). The geocoding of intensity was performed by estimating polynomial coefficients from high correlation points between SAR intensity images and geocoded products of SRTM 1-arcsec DEM and 30 m resolution Landsat Mosaic image (USGS, 2012). In case of ALOS ScanSAR image, each subswath was geocoded, and then merged into a single image by considering the difference of backscattering coefficients between overlaps of geocoded subswath. Each intensity image was calibrated by temporal filtering to suppress speckle noise. Pixel values of ScanSAR 3rd subswath were compared to those of other subswath images within the area of overlap, because the 3rd subswath had a similar incidence angle with FB mode. Based on the overlapped areas between ScanSAR 3rd and 4th subswaths, the calibration factor is applied to other ScanSAR scenes. Orthographic correction of the SAR imagery was deemed unnecessary, because overall topographic gradient within the study region is on the order of 1–3 m (Jones, 2012). Lee filtering (Lee & Pottier, 2009) was

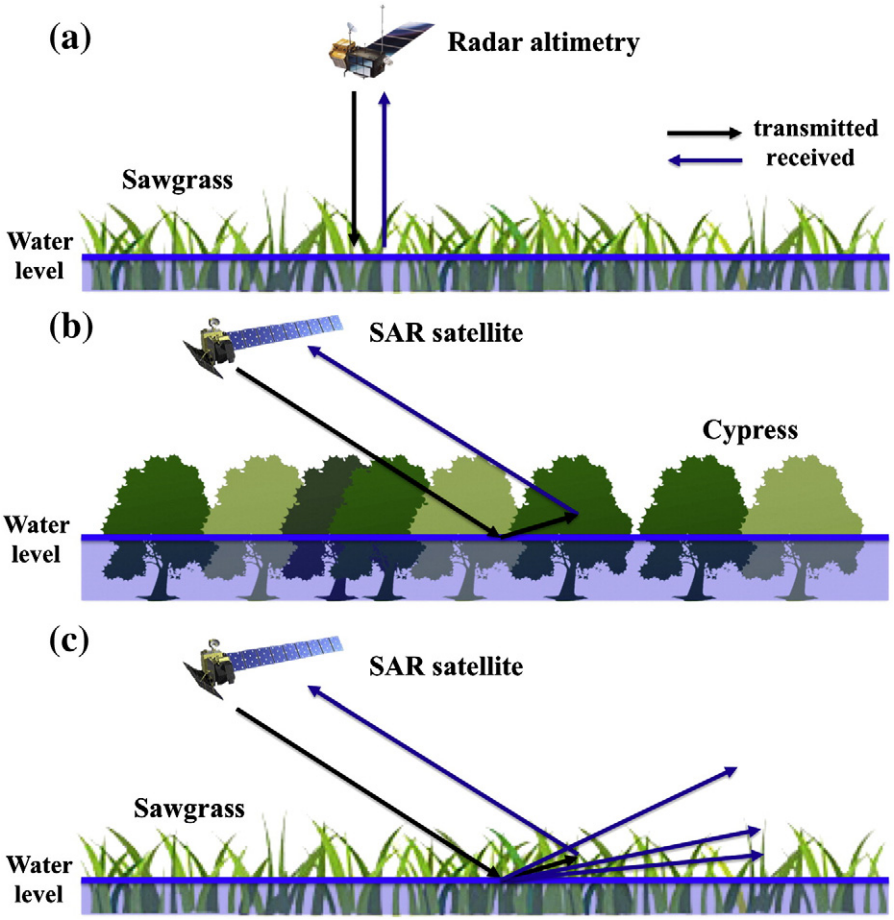

Fig. 3. (a) Nadir observation of Radar altimetry over sawgrass-covered freshwater marsh. (b) Double bounce scattering of SAR signal over swamp forests. (c) Double bounce and surface scattering of SAR return over freshwater marsh (*not to scale*).

applied to the geocoded intensity images to minimize any remaining speckle noise. Finally, filtered intensity images were easily converted into decibel (dB) value corresponding to the backscattering coefficient, which is also called sigma naught (σ_0, dimensionless number).

Sigma naught is affected by physical properties of the radar collection process, such as incidence angle and polarization, and the characteristics of target surface within a resolution element. As incidence angle increases from nadir observation (Fig. 3(a)), the radar backscatter from a ground element gradually decreases. Given high incidence

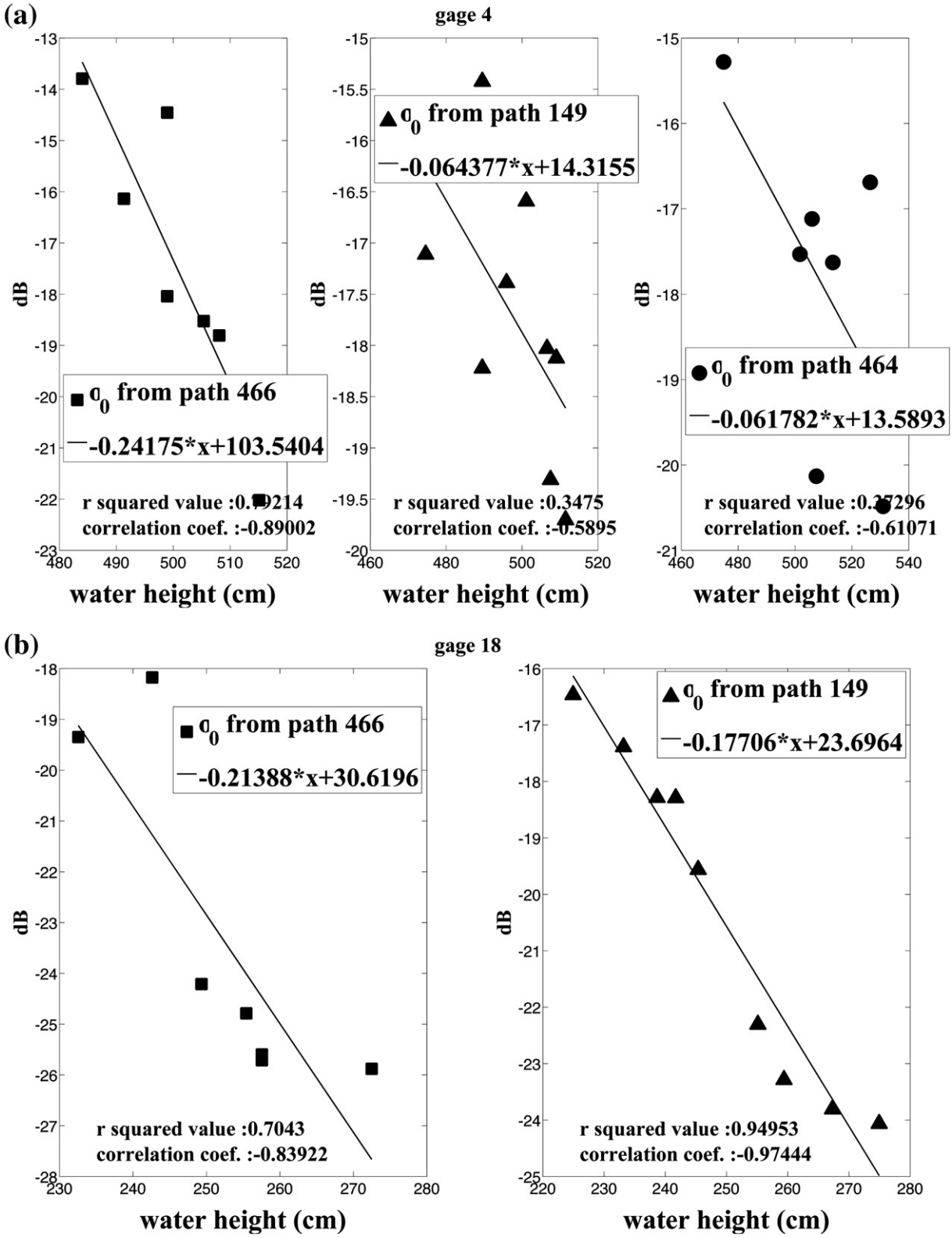

Fig. 4. Comparison between ALOS PALSAR backscattering coefficients from paths 466 (ScanSAR), 149 (Fine), and 464 (Fine) and water height from gage Nos. 4 (a), 18 (b), 22 (c), 23 (d), 30 (e), and 37 (f). Red and blue triangles show decibel from SAR intensity and water height at gages in the location. Each solid line represents linearly fit line from two components, and r squared value and correlation coefficient indicates the strength of linear relationship.

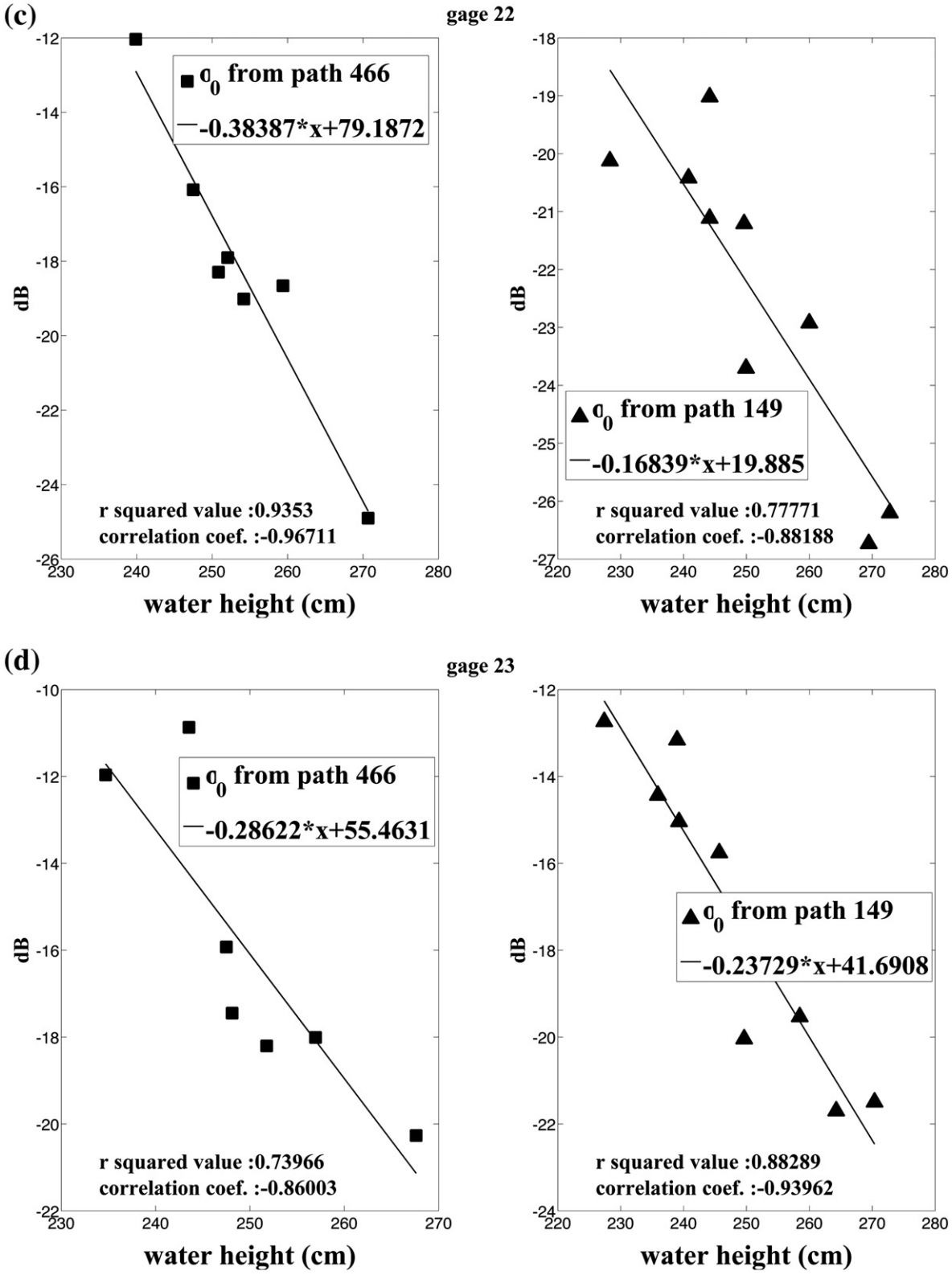

Fig. 4 (*continued*).

angles and a water substrate, double-bounce scattering is one of the most prominent scattering mechanisms from vegetation-covered wetlands. The radar echo from tree trunks provokes backscatter, and the tree trunks function as a corner reflector similar to buildings in urban areas. The vegetation height is a crucial factor that controls the effect of double-bounce scattering. For example, in a freshwater swamp dominated by Cypress that is tens of meters in height, double-bounce scattering becomes enhanced during high water season (Fig. 3(b)). In contrast, the scattering mechanism is weakened over freshwater marsh covered by sawgrass that is only as tall as several meters during

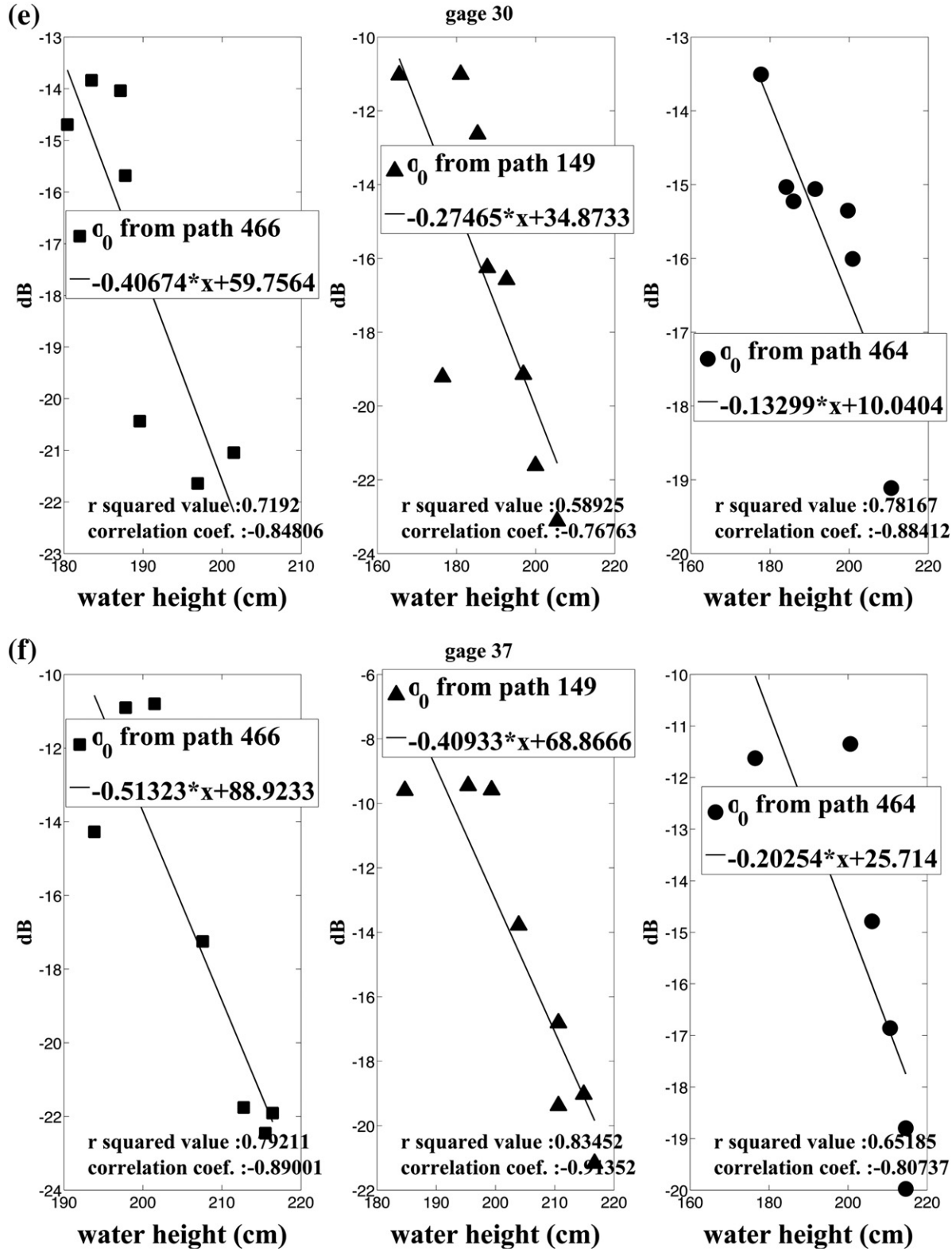

Fig 4 (*continued*).

the same high water period (Fig. 3(c)). Accordingly, the inverse occurs when the height difference between vegetation canopy and water elevation is small. Many radar echoes are reflected away from the radar given surface scattering. Previous studies confirmed that C-band or L-band SAR returns exhibit an inverse relationship with coastal and inland marsh flooding (Ramsey, 1995; Ramsey et al., 2011). However, more study is needed to verify the association between SAR radar backscatter and actual water level from gages. Polarization and wavelength is also an influential factor in double-bounce scattering, and HH-polarized L-band SAR platforms receive the radar echo from flooded wetlands as enhanced by double-bounce scattering. However, the SAR backscatter associated with wetland targets is not simply defined by a single

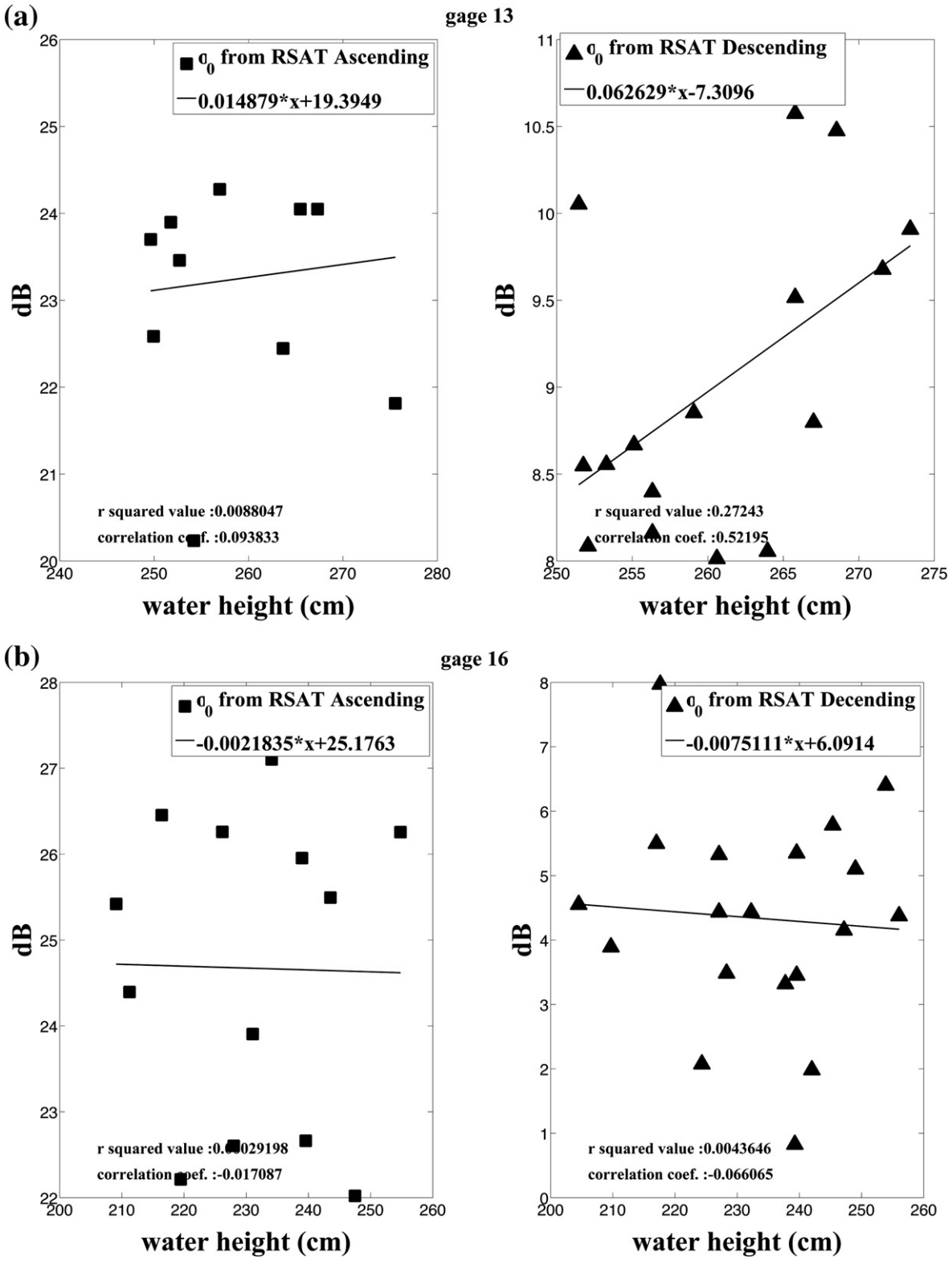

Fig. 5. Comparison between Radarsat-1 backscattering coefficients from ascending and descending track and water height from gage Nos.13 (a), and 16 (b). Red and blue triangles show decibel from SAR intensity and water height at gages in the location. Each solid line represents linearly fit line from two components, and r squared value and correlation coefficient indicates the strength of linear relationship.

parameter. Rather, it is a result of a complicated mixture of soil moisture, biomass, canopy opening, vegetation density, tree height and water surface roughness induced by wind. We hypothesize that water level can be a defining factor of freshwater marsh scattering mechanisms because flooding condition in a short grass gradually converts double-bounce scattering into surface scattering. We expect that parameters of canopy opening and vegetation density that largely affect backscatter in a freshwater swamp are less influential in a freshwater

marsh. Accordingly, exploring the relationship between SAR backscatter coefficient and hydrologic change at gages in the Everglades might help to unravel the elaborate processes of radar backscatter.

4. Results and discussion

4.1. Relationship between SAR backscatter coefficient and water level in the freshwater marshes

The SAR backscatter coefficient is affected by several features of the wetland surface (i.e., the dielectric constant, vegetation type, vegetation density, and water level beneath the vegetation canopy), and radar wavelength and polarization. In the case of swamps (i.e., forested wetlands), high water reinforces double-bounce scattering to amplify the backscatter coefficient. However, water level fluctuations and backscattering coefficients are not highly correlated in swamps. In addition, when water levels increase in forested and herbaceous wetlands, C-band VV polarized SAR backscatter is decreased and the correlation between water level and SAR intensity becomes low (Kasischke et al., 2003). Therefore to-date, water level has been mostly estimated using in-situ gage data, and, backscatter coefficient has only been used to characterize and quantify vegetation distribution or land cover change.

Water levels and backscatter coefficients over herbaceous marshes such as the sawgrass-dominated areas of the Everglades WCAs are highly correlated, when using longer wavelength SAR with horizontal polarization. This relationship is revealed by comparison of SAR backscatter and EDEN gage data. Fig. 4(a)–(f) shows the relationship between water height from multiple gages and backscatter coefficient from ALOS PALSAR intensity images. The inverse linear relationship shows that increased water height lowers the SAR backscatter coefficient from freshwater marshes. These SAR images are from both FB (paths 149 and 464) and ScanSAR (path 466) modes. Backscatter coefficients from paths 149 and 466 produced highly negative correlation coefficients with water height (−0.9 to −0.7). However, products from path 464 generated a relatively lower correlation coefficient than about −0.6. It is difficult to determine the exact cause of this lower correlation, but we suspect that the relatively low number of observations from ALOS PALSAR path 464 given its limited coverage over our interest

Table 2
r-Squared value and correlation coefficient between water height from gages and backscattering coefficients from SAR data.

Gage number	Land cover	ALOS PALSAR						Radarsat-1			
		P466		P149		P464		Ascending		Descending	
		r-Squared	Cor. coef.	r-Squared	Cor. coef.	r-Squared	Cor. coef.	r-Squared	Cor. coef.	r-Squared	Cor. coef.
1	Mixed shrubs	0.030	−0.174	–	–	–	–	0.015	−0.121	–	–
2	Mixed shrubs	0.022	0.150	–	–	–	–	0.000	−0.012	–	–
Mean (mixed shrubs)		0.026	−0.012	–	–	–	–	0.007	−0.066	–	–
Std (mixed shrubs)		0.006	0.229	–	–	–	–	0.010	0.077	–	–
3	Graminoid prairie	0.822	−0.906	0.006	−0.079	0.165	−0.406	–	–	0.063	0.251
4	Graminoid prairie	0.792	−0.890	0.348	−0.589	0.373	−0.611	–	–	0.009	0.097
5	Graminoid prairie	0.026	0.160	0.313	−0.560	0.366	0.605	–	–	0.237	−0.486
6	Graminoid prairie	0.172	0.414	0.530	−0.728	0.061	−0.247	–	–	0.796	−0.892
9	Graminoid prairie	0.848	−0.921	0.505	−0.710	0.367	−0.606	–	–	0.001	−0.031
12	Graminoid prairie	0.000	0.021	0.115	−0.338	0.008	0.090	–	–	0.043	−0.208
13	Graminoid prairie	0.586	−0.766	0.322	−0.567	–	–	0.009	0.094	0.272	0.522
14	Graminoid prairie	0.505	−0.710	0.145	−0.381	0.000	0.006	–	–	0.675	−0.821
15	Graminoid prairie	0.674	−0.821	0.798	−0.894	–	–	0.066	−0.258	–	–
16	Graminoid prairie	0.702	−0.838	0.550	−0.741	–	–	0.000	−0.017	0.004	−0.066
18	Graminoid prairie	0.704	−0.839	0.950	−0.974	–	–	0.099	−0.314	0.099	−0.314
20	Graminoid prairie	0.211	−0.459	0.593	−0.770	–	–	0.281	−0.530	–	–
21	Graminoid prairie	0.424	−0.651	0.818	−0.904	–	–	0.004	0.065	0.231	−0.481
22	Graminoid prairie	0.935	−0.967	0.778	−0.882	–	–	0.537	−0.733	0.274	−0.524
23	Graminoid Prairie	0.740	−0.860	0.883	−0.940	–	–	0.500	−0.707	0.095	−0.309
24	Graminoid prairie	0.802	−0.896	0.756	−0.869	–	–	0.130	−0.360	0.337	0.581
26	Graminoid prairie	0.842	−0.918	0.695	−0.834	–	–	0.097	0.311	–	–
28	Graminoid prairie	0.686	−0.828	0.855	−0.925	–	–	0.056	−0.236	0.203	0.450
29	Graminoid prairie	0.212	−0.461	0.299	−0.546	–	–	0.279	−0.528	0.207	0.455
Mean (graminoid prairie)		0.562	−0.639	0.540	−0.696	0.191	−0.167	0.171	−0.268	0.222	−0.111
Std (graminoid prairie)		0.298	0.404	0.286	0.240	0.174	0.437	0.187	0.330	0.229	0.473
7	Sawgrass	0.741	−0.861	0.521	−0.722	0.719	0.848	–	–	0.255	0.505
8	Sawgrass	0.583	−0.764	0.283	−0.532	0.232	−0.482	–	–	0.039	−0.197
10	Sawgrass	0.681	−0.825	0.759	−0.871	0.318	−0.564	–	–	0.009	0.092
11	Sawgrass	0.490	−0.700	0.638	−0.799	0.849	−0.922	–	–	0.229	0.478
17	Sawgrass	0.924	−0.961	0.483	−0.695	–	–	–	–	0.104	0.322
19	Sawgrass	0.772	−0.878	0.957	−0.978	–	–	0.029	−0.171	–	–
25	Sawgrass	0.039	−0.196	0.249	−0.499	–	–	0.008	0.087	–	–
27	Sawgrass	0.176	0.419	0.253	0.503	0.106	−0.325	–	–	0.489	0.699
30	Sawgrass	0.719	−0.848	0.589	−0.768	0.782	−0.884	–	–	0.201	0.448
31	Sawgrass	0.696	−0.834	0.518	−0.720	0.689	−0.830	0.079	0.281	0.219	0.468
32	Sawgrass	0.444	0.666	0.095	−0.309	0.077	−0.277	0.007	0.082	0.666	0.816
33	Sawgrass	0.763	−0.874	0.485	−0.696	0.619	−0.787	0.583	−0.763	0.017	0.130
34	Sawgrass	0.891	−0.944	0.278	−0.527	0.118	−0.343	–	–	0.309	0.556
35	Sawgrass	0.569	−0.754	0.700	−0.837	0.498	−0.706	–	–	0.009	−0.093
36	Sawgrass	0.535	−0.732	0.580	−0.762	0.023	−0.153	0.009	0.096	0.025	0.159
37	Sawgrass	0.792	−0.890	0.835	−0.914	0.652	−0.807	0.011	−0.103	0.137	0.370
38	Sawgrass	0.414	−0.643	0.546	−0.739	0.081	0.285	0.156	0.394	0.425	0.652
Mean (sawgrass)		0.602	−0.625	0.516	−0.639	0.383	−0.355	0.110	−0.012	0.209	0.360
Std (sawgrass)		0.238	0.474	0.230	0.338	0.304	0.499	0.198	0.355	0.197	0.291

areas, and its large incidence angle from the far-range observation both contribute to this correlation. On the other hand, intensity images from paths 466 and 149 exhibited highly negative correlations with water height. The fact that the data of path 466 and 149 are respectively from ScanSAR and FB mode implies that differences in resolution and satellite flight direction of SAR dataset are not contributing factors. While we observe that different data acquisition methods of FB and ScanSAR do not impact the relationship between water levels and backscatter, the SAR wavelength does. Backscatter from the shorter wavelength (5.6 cm) of C-band Radarsat-1 has a much lower correlation coefficient (~−0.1) with gaged water heights than the longer wavelength L-band ALOS data (Fig. 5(a) and (b)). This reaffirms previous findings that suggested that C-band backscatter coefficients do not have meaningful relationship with water level.

Comparisons (Table 2) among backscatter and water level at 38 EDEN gage sites as a function of land cover type (i.e., mixed shrubs, graminoid prairie and sawgrass) and multiple radar configurations (two modes of ALOS PALSAR and Radarsat-1) features that there exists a close relationship between water level and L-band SAR backscatters. Although the number of observations within some land cover classes is low, backscatter and water levels exhibit different relationships as a function of land cover. Low correlations (~−0.1) occurred over mixed shrubs. These wetland areas have conditions similar to swamp forests, in which woody stems contribute to non-proportional scattering characteristics between radar backscatter and water level. However, for the graminoid and sawgrass marshes, backscatter coefficients from ALOS PALSAR images produce relatively high mean r-squared values of approximately 0.5–0.6 and correlation coefficients of −0.69 to −0.63 in path 466 (ScanSAR) and 149 (FB). Thus we see that two different vegetation types of graminoid prairie dominated by cattail and sawgrass do not have a large effect on the relationship between backscatter coefficients and water height, while radar-operating band has a major impact on this relationship (Figs. 4 and 5: r-squared values 0–±0.3). Scattering mechanisms between C-band radar signal and target surface are not dominated by the single source of water level change, but instead are affected by multiple sources including vegetation composition.

The L-band radar signal from ALOS PALSAR appears to be largely influenced by water level beneath vegetation in Everglades marshes. However, other factors such as seasonal variation in vegetation cover may still influence backscatter. High and negative correlations (−0.7 to −0.6) between water level and backscatter from ALOS PALSAR paths 466 and 149 as averaged by SAR acquisition date continue to suggest that it is possible to estimate water height from L-band SAR backscatter coefficients. The backscatter coefficient of both fine-beam and ScanSAR mode SAR data is linearly decreased (Fig. 6). However, large variations in backscatter coefficient (standard deviation of about 3 dB) within SAR acquisitions suggest that there are limits to high-accuracy water height estimation using only SAR backscatter coefficient given complicated wetland conditions.

Nearly 80% of the annual precipitation in the Everglades occurs in the wet season (May to October) and often drought conditions prevail in the dry season (November to April). In most years, water level reaches its peak in the fall (September) while lowest levels occur during spring (March and April) (Kasischke et al., 2003). The water levels measured at the inland EDEN gages followed this annual cycle (Fig. 7(a)) (However drought conditions may result in no standing water where our technique would not work as was seen in the 2009 dry season). Given the mean water level at inland water gages and backscatter coefficient from path 149 between late 2009 and early 2011 (Fig. 7(b)), increased or peaked water levels reduce the backscatter coefficient in the freshwater marshes (sawgrass and graminoid prairie). That is, the backscatter coefficient in the marshes tends toward the opposite direction of water level changes. Seasonal variation of the backscatter coefficient is largely affected by hydrologic variation, not biomass, soil moisture, or phenologic changes in vegetation. It is important to note that in this

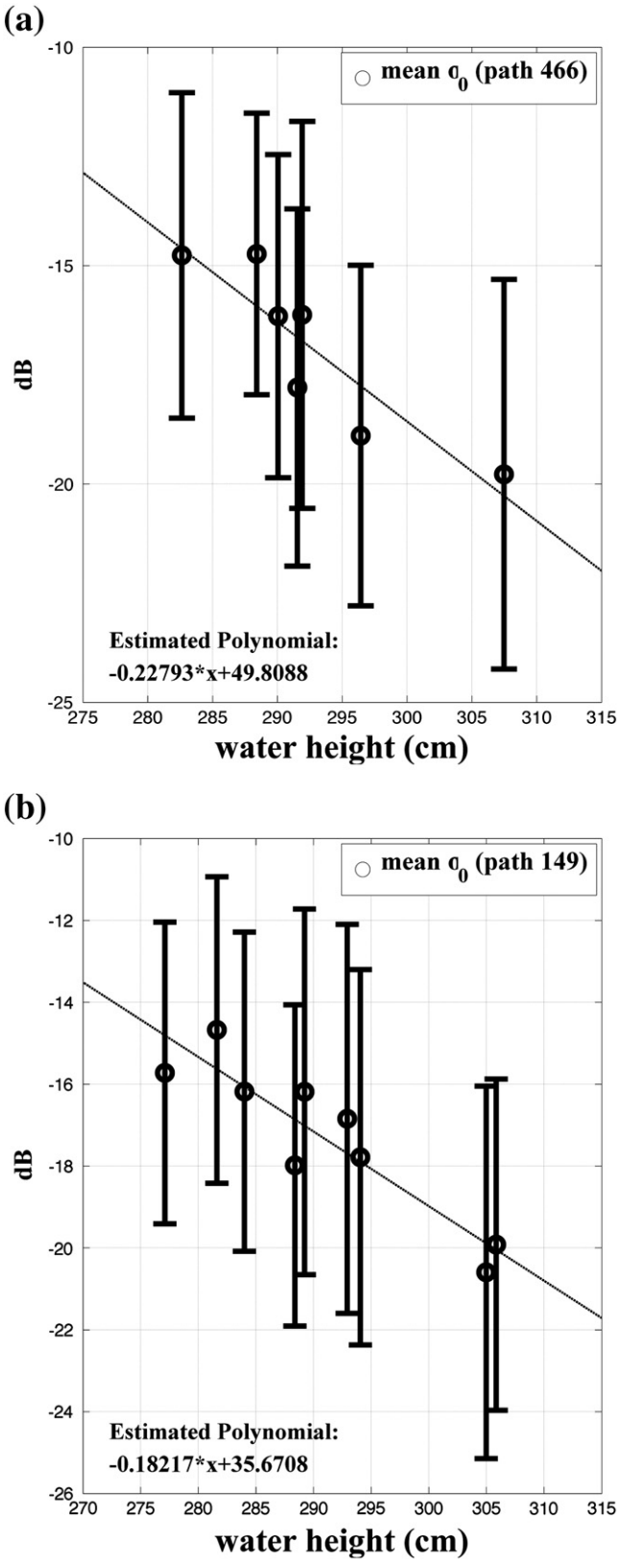

Fig. 6. Mean backscattering coefficient ((a) paths 466 and (b) 149) and water height from each SAR date. Black circles represent averaged backscatter coefficient and length of error bars mean a standard deviation. Dotted lines are a linearly fit line from mean backscatter coefficient and water height.

regarding the Everglades may present a best-case condition in terms of water level variation as a dominant scattering mechanism. Leaf-on and leaf-off conditions of grasses in Everglades marshes may not have

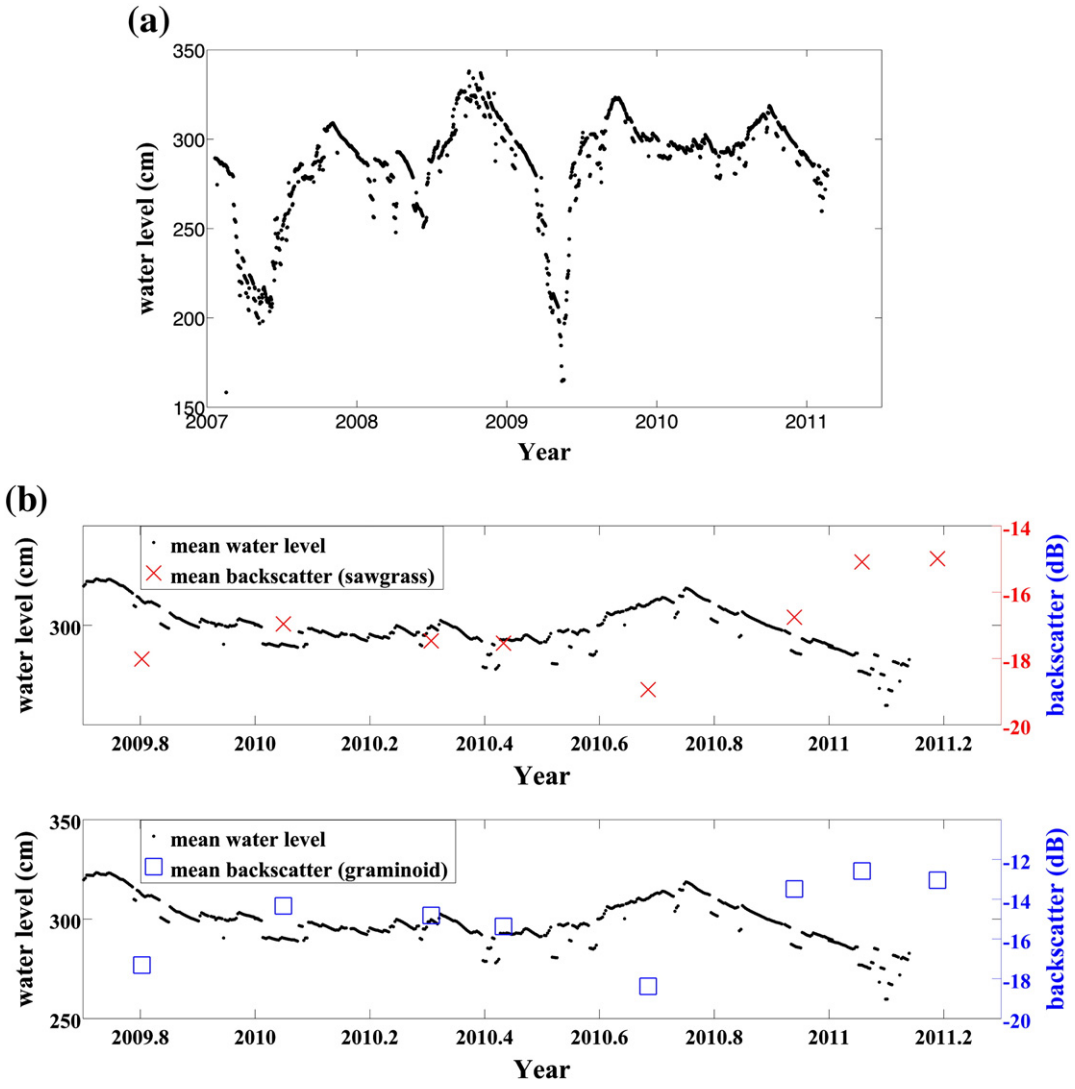

Fig. 7. (a) Mean water level from wetland water level gages in the freshwater marshes of sawgrass and graminoid prairie between 2007 and early 2011. (b) Mean water level from wetland water level gages and mean backscatter coefficient of sawgrass (red cross) and graminoid prairie (blue squares) marshes between late 2009 and early 2011.

as strong a seasonal component or as large an impact on the scattering of long wavelength radar signal than might be the case in other more temperate herbaceous wetlands.

4.2. Relationship between interferometric phase, backscattering coefficients, and water level changes over the wetlands

Hydrologic variations in wetlands affect the phase of interferograms (Wdowinski et al., 2004, 2008) as well as the backscatter coefficients of geocoded SAR scenes from C- and L-band SAR sensors. Therefore the notable effect results in spatially similar color changes in a wrapped PALSAR interferogram (Fig. 8(a)) and the backscatter difference (Fig. 8(b)). When the interferogram was generated from a pair with relatively small perpendicular baseline (~500 m) and temporal baseline (46 days for ALOS PALSAR), high coherence is maintained over many regions of wetlands (Fig. 8(a)). However, the density and type of vegetation affect the inconsistent scattering and weak double-bounce scattering in freshwater marsh such as WCA 2 and 3A-3 (Fig. 8(a)), and the coherence is declined to low level below 0.2. When the temporal baseline of InSAR pairs over the freshwater marsh is longer than a critical date (46 days) or the perpendicular baseline is large (>700 m), the interferograms rarely exhibit good coherence. For these reasons, InSAR pairs covering freshwater marsh require strong filtering to implement reliable phase unwrapping.

The number of InSAR pairs with ideal conditions of small temporal and spatial baselines is restricted. Furthermore, ScanSAR–ScanSAR interferometry from ALOS PALSAR is not often feasible, because the bursts of ScanSAR are not fully synchronized in a revisiting date. The misalignment results in total decorrelation of SAR interferograms. However, in such formidable cases, our results suggest that difference of backscatter coefficients could help to estimate spatial water level change, replacing inadequate interferograms to a certain degree. The differencing of backscatter coefficients and wrapped interferogram from a pair of PALSAR ScanSAR image from September, 13, 2010 and January, 29, 2011 shows similar patterns of changes (Fig. 9). This is especially evident in WCA 2. The SAR pair has a perpendicular baseline of 426.65 (m), and PALSAR ScanSAR–ScanSAR interferometry is available due to the synchronization of SAR bursts meaning enough overlaps between SAR observations. The burst synchronization is very rarely happening in PALSAR ScanSAR, and the other pair of July, 29, 2010 and September, 13, 2010 (Fig. 9) does not generate a proper interferogram due to the loss of coherence. The difference of backscatter coefficient is always available, and approximate water level changes within wetlands of the Everglades can be estimated from differences in ScanSAR backscatter coefficients (lowest part of Fig. 9).

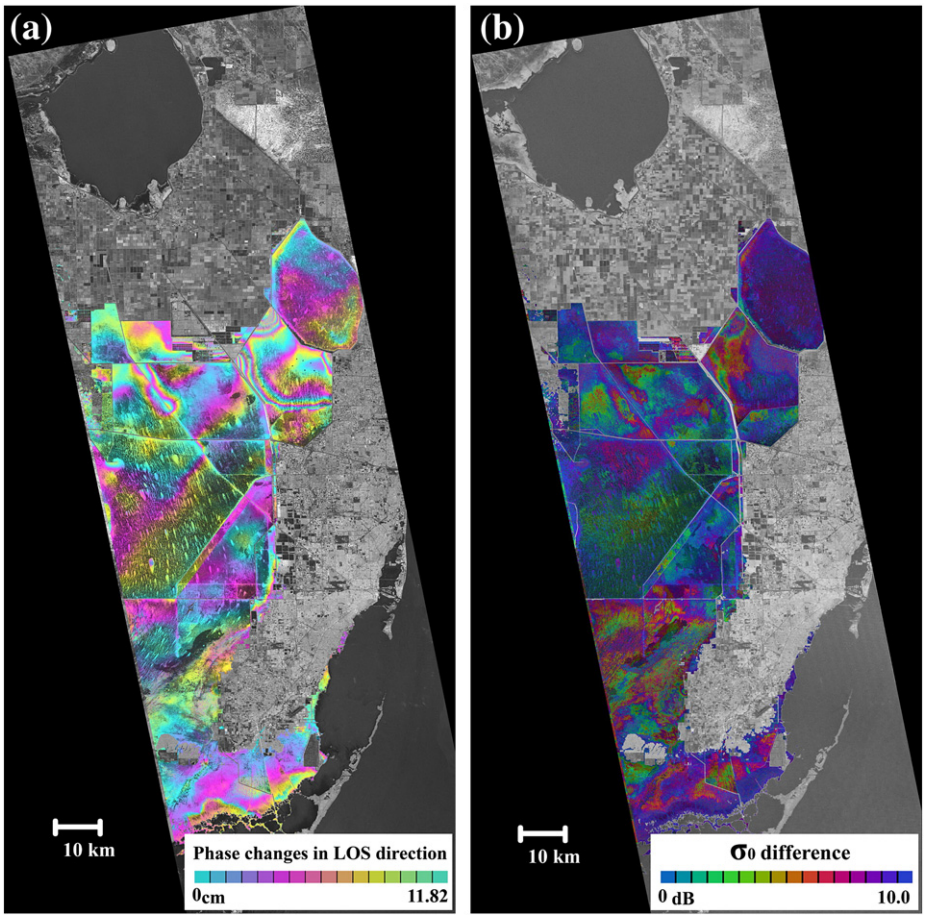

Fig. 8. (a) Wrapped interferogram from ALOS PALSAR SAR data and (b) difference of ALOS PALSAR fine-beam mode backscatter coefficients in the Everglades, Florida, between 2010.04.21 and 2010.06.06 (period of transition between dry and wet seasons; Cyclically colored by 10.0 dB to allow comparison with the wrapped interferogram). Due to inverse relationship of hydrologic change and backscatter in the marshes, panels (a) and (b) show similar pattern of spatial color change.

4.3. Complementarity of InSAR and SAR backscatter coefficient to estimate water level changes in the wetlands

The complementary uses of unwrapped interferometric phases and difference of backscatter coefficients are highlighted through their comparison with water level at EDEN gages (Fig. 10). Unwrapped interferometric phases from two SAR pairs (red crosses) are sparser than differences of backscatter coefficients (blue dot) in the figure, because only high coherence pixels from an interferogram were unwrapped by avoiding errors by phase jumps. As water levels increase both unwrapped interferometric phases and difference of backscatter coefficient are decreased. It is the nature of interferometric phases that increases in water level decreases the relative distance between satellite and target as well as phase difference between nearby pixels of an unwrapped interferogram. Therefore, it makes sense that water level changes and unwrapped phase are highly correlated (Fig. 10(a) and (b)). Although water level change and difference of backscatter coefficients are relatively less correlated, the two parameters have an inverse linear relationship to a certain degree. It is possible to estimate water level changes at specific locations of freshwater marsh from differences in backscatter coefficient, in places or at times when L-band SAR interferometry is not possible.

Use of backscatter coefficient and its differencing is not a perfect substitute for interferometry. InSAR can be rather used for deriving the reference water level change to obtain absolute water level change within the freshwater marsh as the fusion of radar altimetry and InSAR technology can be utilized for absolute water level change within swamp forests (Kim et al., 2009). Unfortunately, in the Everglades, the radar altimetry does not cross the major wetlands of the water conservation area or the Everglades National Park. Furthermore, while gage data have been used with InSAR for detailed estimation of water level changes, gages may often fall in the low coherence areas, making the combination of gage data and InSAR infeasible. However, because of a close relationship between L-band radar backscatter and water level in the freshwater marsh, the hydrologic change estimated from the backscatter coefficient can be used for a reference water level change (Kim, Hong, & Won, 2005).

We used two pairs from FB interferometry (2010.04.21–2010.06.06) and ScanSAR–ScanSAR interferometry (2010.09.13–2011.01.29) to test this possibility combining the InSAR pair and the backscatter coefficient for this purpose. Two wrapped differential SAR interferograms were unwrapped using the minimum cost flow (MCF) algorithm, while excluding low-coherence area with values smaller than 0.2. In each section of water conservation area, the data with the highest r-squared value at the location of wetland gages (Table 2) was used. And, the linear fitted equations between water level and backscatter coefficient were utilized for estimating hydrologic change in the SAR acquisition dates. The estimated water level and its subtraction between two SAR acquisition dates are approximated as water level change during the period of the InSAR pair, which represents high-resolution water level change within wetlands. The integration of unwrapped InSAR pair and a reference water level change at gages was validated using other

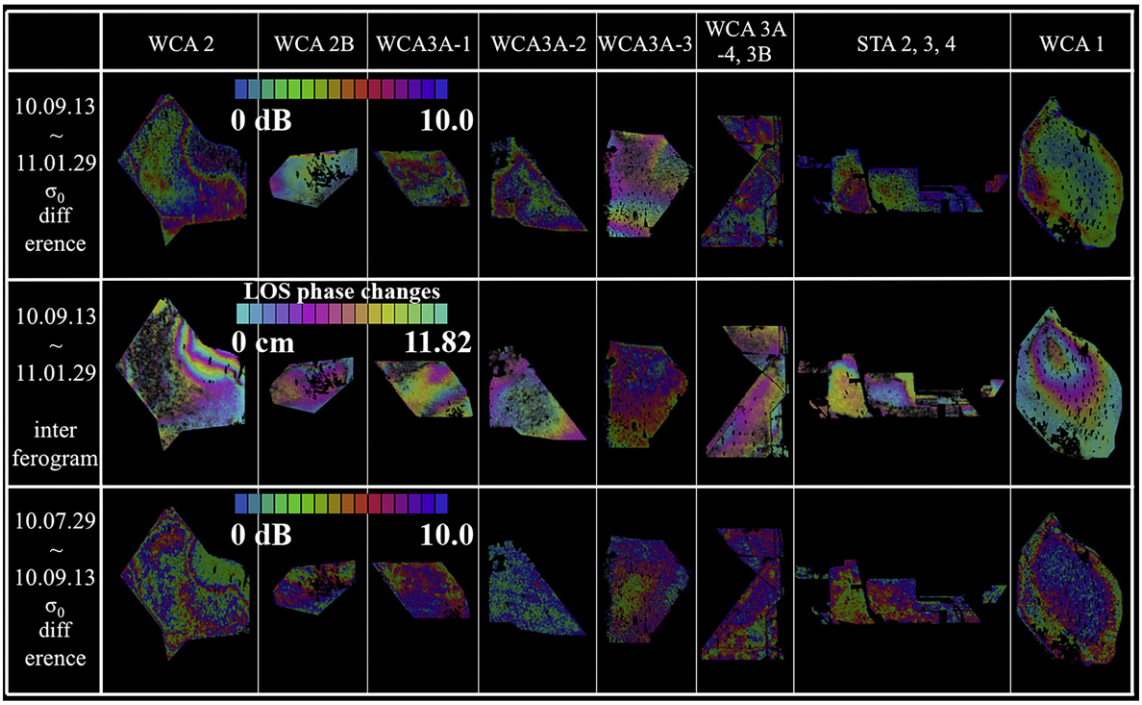

Fig. 9. Difference of backscatter coefficient and wrapped interferogram over each section of Water Conservation Areas and Stormwater Treatment Areas from two ALOS ScanSAR pairs, 2010.09.13–2011.01.29 and 2010.07.29–2010.09.13. And, an interferogram from one pair, 2010.07.29 and 2010.09.13, is missing, because ScanSAR-ScanSAR interferometry is not available due to a burst misalignment.

wetland gages. Each section of water conservation area shows a different magnitude of water level change, because the segments are dissected by levees or canals (Jones et al., 2012) (Fig. 11). The spatial hydrologic change is induced by the sensitivity of InSAR to the movement of the water surface. The low-coherence area was not included in the generation of absolute water level change map to avoid the phase jumps and inaccurate reconstruction of actual water level change. When the wetland gages (WCA 1 for Fine pair and WCA 1, 2, and 3A-2 for ScanSAR pair) are located in the low-coherence region, the closest point (within 3 pixels; approximately 100 m) of interferograms is used for the integration (Table 3). Also, because there is no available wetland gage data for STA, the section was not included in Fig. 11. The accuracy varies along with each section, and the range is between 1.27 cm and 6.30 cm. Furthermore, there is no significant difference

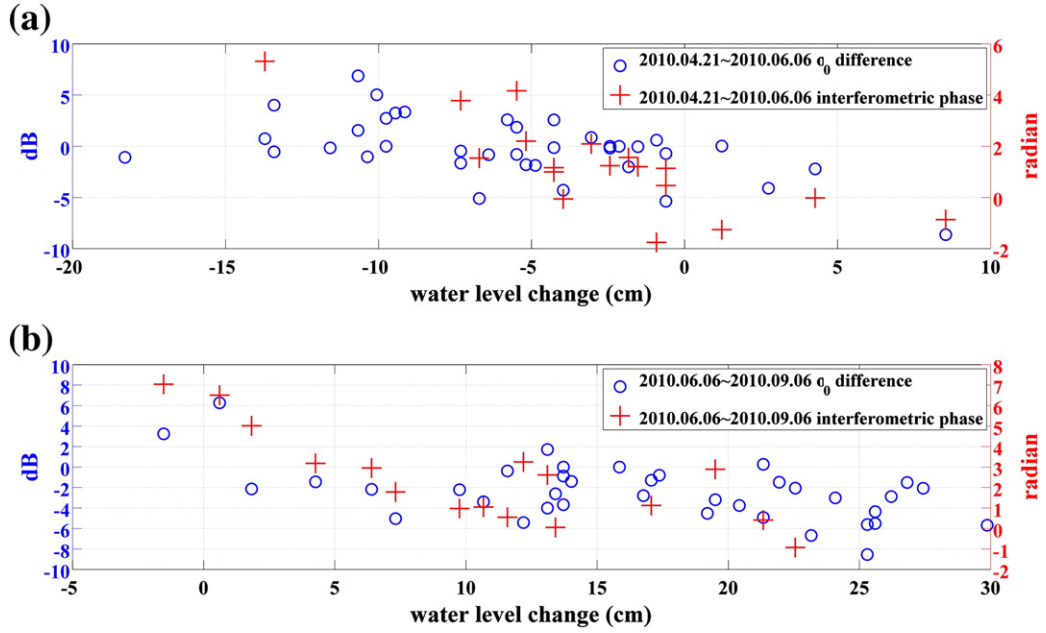

Fig. 10. Comparison of difference of backscattering coefficient and unwrapped interferometric phase between (a) 2010.04.21 and 2010.06.06 and (b) 2010.06.06 and 2010.09.06. Blue circles are from difference of SAR intensity and its dimension is decibel. And, red crosses are from unwrapped interferometric phase and its dimension is radian.

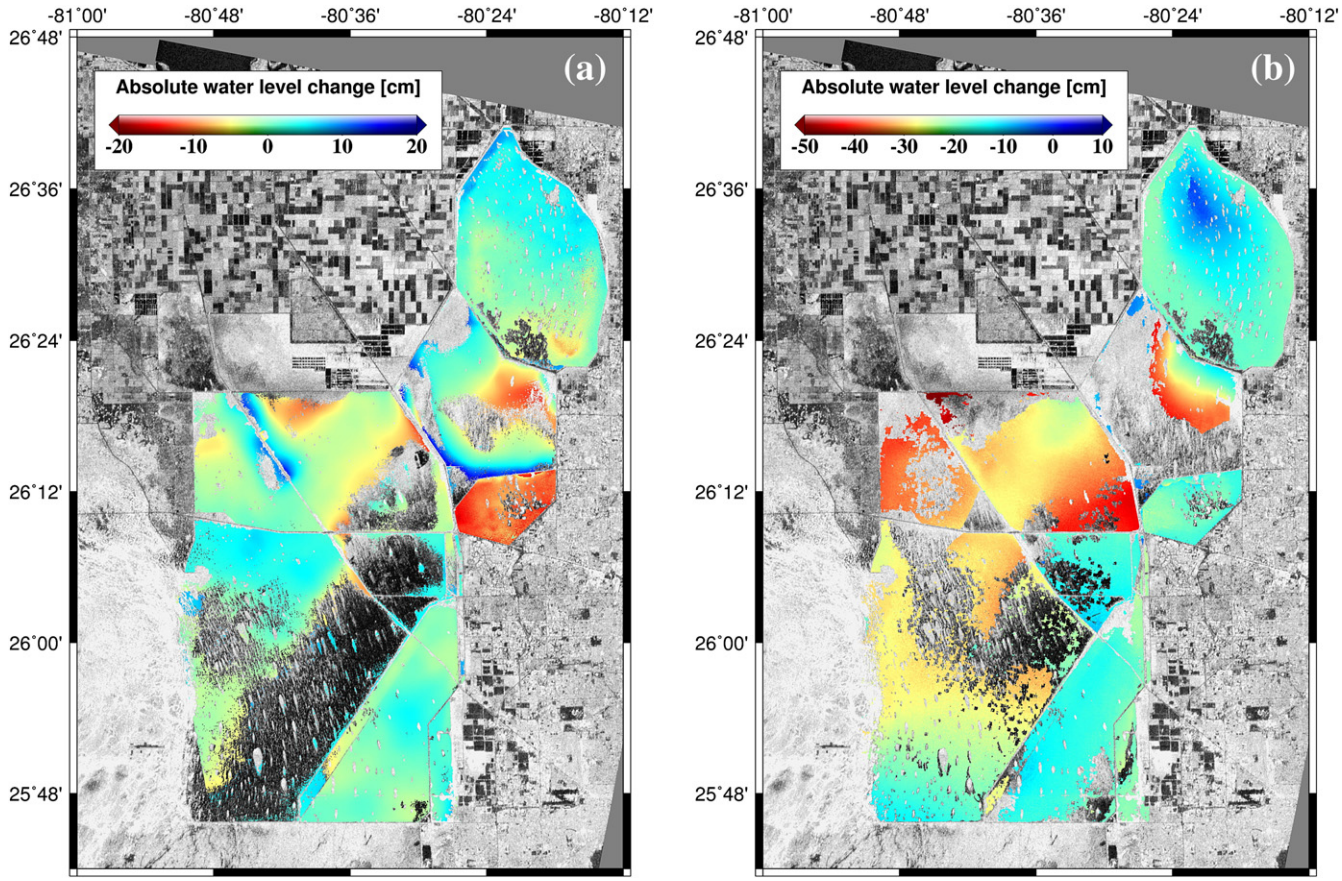

Fig. 11. Absolute water level change using ALOS PALSAR InSAR pair ((a) fine-beam mode 2010.04.21–2010.06.06, (b) ScanSAR mode 2010.09.13–2011.01.29) and reference water level change estimated from the relationship between backscatter coefficient and water level measured in wetland water level gages.

between two SAR observation modes acquired from descending and ascending tracks. The results suggest that the integration of SAR intensity and phase information to estimate absolute water level change is feasible. Also, the different conditions of each section in water conservation area, such as biomass and density, affect the accuracy for the integration. A long history of L-band backscatter coefficient in the freshwater marsh can enhance the accuracy because of improved derivation of linear relationship between radar backscatter and water level.

Table 3
Combined InSAR pairs and SAR backscattering coefficient validated at multiple water gages within wetlands. ("–" means that there is no available gage data due to low coherence).

Period	Beam mode	Section	RMSE (cm)
2010.04.21–2010.06.06	Fine	WCA 2	–
2010.04.21–2010.06.06	Fine	WCA 2B	2.5421
2010.04.21–2010.06.06	Fine	WCA 3A-1	6.2981
2010.04.21–2010.06.06	Fine	WCA 3A-2	1.2726
2010.04.21–2010.06.06	Fine	WCA 3A-3	3.9526
2010.04.21–2010.06.06	Fine	WCA 3A-4, 3B	2.3423
2010.04.21–2010.06.06	Fine	WCA 1	2.6158
2010.09.13–2011.01.29	ScanSAR	WCA 2	–
2010.09.13–2011.01.29	ScanSAR	WCA 2B	2.8023
2010.09.13–2011.01.29	ScanSAR	WCA 3A-1	4.7518
2010.09.13–2011.01.29	ScanSAR	WCA 3A-2	–
2010.09.13–2011.01.29	ScanSAR	WCA 3A-3	1.3665
2010.09.13–2011.01.29	ScanSAR	WCA 3A-4, 3B	3.7117
2010.09.13–2011.01.29	ScanSAR	WCA 1	1.5403

5. Conclusions

The adaptive management of Everglades restoration requires efficient and accurate monitoring of wetland hydrology at the highest temporal and finest spatial resolutions possible. Many investigations have worked to develop methods of combining the EDEN gage network with radar remote sensing technology to understand Everglades wetland hydrology. However, few have explored relationships among hydrologic variation and SAR backscatter coefficients.

We combined ALOS PALSAR L-band and Radarsat-1 C-band data with daily mean water heights derived from the EDEN to compare SAR backscatter coefficients and Everglades water levels. While the various wavelengths and polarizations of these sensors are affected differently by various potential scattering mechanisms, we found that L-band SAR backscatter coefficients are closely related to water level in freshwater marshes of the Everglades. C-band radar does not produce a reasonable relationship with the fluctuation of water level, because components other than hydrologic change, such as vegetation composition, structure and density affect the radar backscattering. L-band backscatter coefficients in the freshwater marsh of the Everglades are dominated by the single factor of water level fluctuation. Therefore, approximate water level can be estimated from L-band SAR backscatter coefficients.

SAR interferometry provides detailed hydrologic information when coherence is maintained and interferometric phases are able to unveil relative water level changes between particular dates. However, low coherence often occurs in the InSAR pairs with large temporal and spatial baseline or without enough double-bounce scattering. Comparison with interferograms, which were assumed to provide measures of real spatial water level change, made it clear that hydrologic changes affect the

difference of backscatter coefficients as well as interferometric phase. Integrating water level change derived from L-band backscatter and InSAR pairs can estimate absolute water level change in the freshwater marsh. The accuracy of absolute water level change estimated from our integration of FB and ScanSAR mode ALOS PALSAR data, suggests that meaningful hydrologic monitoring is possible. Further, it may be feasible and appropriate to use L-band SAR backscatter coefficients in place of SAR interferometry when low coherence disturbs the generation of a proper interferograms or ScanSAR–ScanSAR interferometry is not available.

Although our research shows that SAR backscatter coefficients can be useful for understanding wetland hydrology in the Everglades, it should be recognized that SAR intensity data is noisy and backscatter coefficients still include numerous effects of non-hydrological changes. Even well-known filtering techniques of lee, gamma, frost, and median filter cannot eliminate all the noise. And, it is not easy to distinguish hydrologic change signatures from others such as seasonal variation of vegetation and weather conditions. Thus, better filtering of SAR intensity and discriminating water level changes on backscatter coefficients from others and understanding the role of additional parameters, such as wind on water backscatter properties (Braggs scattering), requires a further study. For all these reasons, broader application of radar backscatter coefficient analysis for the purpose of mapping temporal and spatial changes in Everglades wetland water levels is feasible.

References

Alsdorf, D., Melack, J., Dunne, T., Mertes, L., Hess, L., & Smith, L. (2000). Interferometric radar measurements of water level changes on the Amazon floodplain. *Nature*, *404*, 174–177.

Alsdorf, D., Smith, L., & Melack, J. (2001). Amazon floodplain water level changes measured with interferometric SIR-C radar. *IEEE Transactions on Geoscience and Remote Sensing*, *39*, 423–431.

Amelung, F., Galloway, D. L., Bell, J. W., Zebker, H. A., & Laczniak, R. L. (1999). Sensing the ups and downs of Las Vegas–InSAR reveals structural control of land subsidence and aquifer-system deformation. *Geology*, *27*(6), 483–486.

Betbeder, J., Gond, V., Frappart, F., Baghdadi, N., Briant, G., & Bartholome, E. (2014). Mapping of Central Africa forested wetlands using remote sensing. *IEEE Journal of Selected Topics on Earth Observation and Remote Sensing*, *7*(2), 531–542. http://dx.doi.org/10.1109/JSTARS.2013.2269733.

Casu, F., Buckley, S. M., Manzo, M., Pepe, A., & Lanari, R. (2005). Large scale InSAR deformation time series: Phoenix and Houston case studies. *Proceedings of the IEEE International Geoscience Remote Sensing Symposium*(7), 5240–5243.

Curlander, J. C., & McDonough, R. N. (1991). *Synthetic aperture radar — Systems and signal processing*. New York: John Wiley & Sons.

Doren, R. F., Rutchey, K., & Welch, R. (1999). The Everglades: A perspective of the requirements and applications for vegetation map and database products. *Photogrammetric Engineering & Remote Sensing*, *65*(2), 155–161.

Douglas, M. S. (1947). *The Everglades: River of grass*. New York: Plenum Press.

Frappart, F., Seyler, F., Martinez, J. M., León, J. G., & Cazenave, A. (2005). Floodplain water storage in the Negro River basin estimated from microwave remote sensing of inundation area and water levels. *Remote Sensing of Environment*, *99*, 387–399. http://dx.doi.org/10.1016/j.rse.2005.08.016.

Fraser, L. H., & Keddy, P. A. (2005). *The world's largest wetlands: Ecology and conservation*. Cambridge University Press.

Galloway, D. L., & Hoffmann, J. (2007). The application of satellite differential SAR interferometry-derived ground displacements in hydrogeology. *Hydrogeology Journal*, *15*(1), 133–154. http://dx.doi.org/10.1007/s10040-006-0121-5.

Hanssen, R. F. (2000). *Radar interferometry: Data interpretation and error analysis*. Kluwer Academic Publishers.

Hess, L. L., Melack, J. M., Filoso, S., & Wang, Y. (1995). Delineation of inundated area and vegetation along the Amazon floodplain with the SIR-C synthetic aperture radar. *IEEE Transactions on Geoscience and Remote Sensing*, *33*, 896–904.

Hess, L. L., Melack, J. M., Novo, E. M. L. M., Barbosa, C. C. F., & Gastil, M. (2003). Dual-season mapping of wetland inundation and vegetation for the central Amazon basin. *Remote Sensing of Environment*, *87*, 404–428.

Hess, L. L., Melack, J. M., & Simonett, D. S. (1990). Radar detection of flooding beneath the forest canopy: A review. *International Journal of Remote Sensing*, *11*, 313–1325.

Hong, S. -H., Wdowinski, S., Kim, S. -W., & Won, J. -S. (2010). Multi-temporal monitoring of wetland levels in the Florida Everglades using interferometric synthetic aperture radar (InSAR). *Remote Sensing of Environment*, *87*, 404–428.

Jones, J. W. (2011). Remote sensing of vegetation pattern and condition to monitor changes in Everglades biogeochemistry. *Critical Reviews in Environmental Science and Technology*, *41*(S1), 64–91.

Jones, J. W., Desmond, G. B., Henkle, C., & Glover, R. (2012). An approach to regional wetland digital elevation model development using a differential global positioning system and a custom-built helicopter based surveying system. *International Journal of Remote Sensing*, *33*(2), 450–465.

Kasischke, E. S., Smith, K. B., Bourgeau-Chavez, L. L., Romanowicz, E. A., Brunzell, S., & Richardson, C. J. (2003). Effects of seasonal hydrologic patterns in south Florida wetlands on radar backscatter measured from ERS-2 SAR imagery. *Remote Sensing of Environment*, *88*, 423–441.

Kim, S. -W., Hong, S. -H., & Won, J. -S. (2005). An application of L-band synthetic aperture radar to tide height measurement. *IEEE Transactions on Geoscience and Remote Sensing*, *43*(7), 1472–1478.

Kim, J. -W., Lu, Z., Lee, H., Shum, C. K., Swarzenski, C. M., Doyle, T. W., et al. (2009). Integrated analysis of PALSAR/Radarsat-1 InSAR and ENVISAT altimeter data for mapping of absolute water level changes in Louisiana wetlands. *Remote Sensing of Environment*, *113*(11), 2356–2365. http://dx.doi.org/10.1016/j.rse.2009.06.014 (ISSN 0034-4257).

Kim, S. -W., Wdowinski, S., Amelung, F., Dixon, T. H., & Won, J. -S. (2014s). Interferometric coherence analysis of the Everglades wetlands, south Florida. *IEEE Transactions on Geoscience and Remote Sensing* (in press).

Kwoun, O. -I., & Lu, Z. (2009). Multi-temporal RADARSAT-1 and ERS backscattering signatures of coastal wetlands in southeastern Louisiana. *Photogrammetric Engineering & Remote Sensing*, *75*(5), 607–617.

Lee, S. -K., Hong, S. -H., Kim, S. -W., Yamaguchi, Y., & Won, J. -W. (2006). Polarimetric features of oyster farm observed by AIRSAT and JERS-1. *IEEE Transactions on Geoscience and Remote Sensing*, *44*(10), 2728–2735.

Lee, J. -S., & Pottier, E. (2009). *Polarimetric radar imaging: From basics to applications*. Boca Raton, FL: CRC Press.

Liu, G., Buckley, S. M., Ding, X., Chen, Q., & Luo, X. (2009). Estimating spatiotemporal ground deformation with improved permanent-scatter radar interferometry. *IEEE Transactions on Geoscience and Remote Sensing*, *47*(8), 2762–2772.

Lu, Z. (2007). InSAR imaging of volcanic deformation over cloud-prone areas — Aleutian Islands. *Photogrammetric Engineering & Remote Sensing*, *73*, 245–257.

Lu, Z., Crane, M., Kwoun, O. -I., Wells, C., Swarzenski, C., & Rykhus, R. (2005). C-band radar observes water level change in swamp forests. *Eos*, *86*, 141–144.

Mitsch, W. J., & Gosselink, J. G. (2007). *Wetlands* (4th ed.). New York: John Wiley & Sons, Inc.

National Research Council (NRC) (2001). *Aquifer storage and recovery in the comprehensive Everglades restoration plan: A critique of the pilot projects and related plans for ASR in the Lake Okeechobee and western Hillsboro areas*. Washington, D.C.: National Academics Press.

Ramsey, E. W., III (1995). Monitoring flooding in coastal wetlands by using radar imagery and ground-based measurements. *International Journal of Remote Sensing*, *16*(13), 2495–2502.

Ramsey, E., III, Lu, Z., Suzuoki, Y., Rangoonwala, A., & Werle, D. (2011). Monitoring duration and extent of storm surge flooding along the Louisiana coast with Envisat ASAR data. *IEEE Journal of Selected Topics in Applied Earth Observations and Remote Sensing*, *4*(2), 387–399.

Rebelo, L. -S. (2010). Eco-hydrological characterization of inland wetlands in Africa using L-band SAR. *IEEE Journal of Selected Topics in Applied Earth Observations and Remote Sensing*, *3*(4), 554–559. http://dx.doi.org/10.1109/JSTARS.2010.2070060.

Smith, L. C. (1997). Satellite remote sensing of river inundation area, stage, and discharge: A review. *Hydrological Processes*, *11*, 1427–1439.

Solecki, W. D., Long, J., Harwell, C. C., Myers, V., Zubrow, E., Ankerson, T., et al. (1999). Human–environment interaction in South Florida's Everglades region: Systems of ecological degradation and restoration. *Urban Ecosystems*, *3*(304), 305–343.

South Florida Ecosystem Restoration Task Force (SFERTF) (1998). *An integrated plan for South Florida ecosystem restoration and sustainability: Success in the making*. The working group of the South Florida ecosystem restoration task force.

South Florida Water Management District (SFWMD) (2004). Land cover land use 2004. http://my.sfwmd.gov/gisapps/sfwmdxwebdc/dataview.asp?query=unq_id=1813 (Accessed 20 July 2011)

Tellis, P. A. (2006). *The Everglades Depth Estimation Network (EDEN) for support of ecological and biological assessments*. U.S. Geological Survey Fact Sheet 2006-3087, 1–4.

Tong, X., Sandwell, D. T., & Fialko, Y. (2010). Coseismic slip model of the 2008 Wenchuan earthquake derived from joint inversion of interferometric synthetic aperture radar, GPS, and field data. *Journal of Geophysical Research*, *115*, B04314. http://dx.doi.org/10.1029/2009JB006625.

U.S. Army Corps of Engineers (USACE) (1999). *The Comprehensive Everglades Restoration Plan (CERP)*. Washington D.C.: Central and Southern Florida Comprehensive Review Study.

U.S. Geological Survey (USGS) (2012). Earth explorer from earth resources observation and science. http://earthexplorer.usgs.gov (Accessed 11 Nov 2011)

Wang, Y., Hess, L. L., Filoso, S., & Melack, J. M. (1995). Understanding the radar backscattering from flooded and nonflooded Amazonian forests: Results from canopy backscatter modeling. *Remote Sensing of the Environment*, *54*, 324–332.

Wdowinski, S., Amelung, F., Miralles-Wilhelm, F., Dixon, T., & Carande, R. (2004). Space-based measurements of sheet-flow characteristics in the Everglades wetland, Florida. *Geophysical Research Letters*, *31*, L15503. http://dx.doi.org/10.1029/2004GL020383.

Wdowinski, S., Kim, S. -W., Amelung, F., Dixon, T., Miralles-Wilhelm, F., & Sonenshein, R. (2008). Space-based detection of wetlands' surface water level changes from L-band SAR interferometry. *Remote Sensing of Environment*, *112*, 681–696.

Zweig, C. L., & Kitchens, W. M. (2008). Effects of landscape gradients on wetland vegetation communities: Information for large-scale restoration. *Wetlands*, *28*(4), 1086–1095.